Numerical Analysis of Laminar Temperature-Stratified Flow in a Horizontal Duct

Yu, Bo
Postdoctoral fellow on leave from Xi'an Jiaotong University

Ozoe, Hiroyuki
Postdoctoral fellow on leave from Xi'an Jiaotong University | Institute of Advanced Material Study Kyushu University

https://doi.org/10.15017/7922

出版情報：九州大学機能物質科学研究所報告. 14 (2), pp.111-117, 2000-12-25. Institute of Advanced Material Study Kyushu University
バージョン：
権利関係：

Numerical Analysis of Laminar Temperature-Stratified Flow in a Horizontal Duct

Bo YU* and Hiroyuki OZOE

Numerical simulations were performed for the laminar temperature-stratified flow in a horizontal duct. MINMOD scheme was applied to approximate the convection term in the governing equations. The studies were made for both water and air. Both the transient process and steady stratified flow patterns are reported. The effects of the Grashof number, Prandtl number and aspect ratio (length/width) on the flow motion were studied.

Introduction

Temperature stratified flow in a duct is often encountered among others in combustion processes in a tunnel, emission processes of industrial pollutant. This flow pattern is very important, but the reports on it are still very few. Some of the reports are: Ozoe et al. [1,2] originally studied both experimentally and numerically the transient process of water in a rectangular duct with an aspect ratio of 2. Mo. et al. [3] reported the transient formation process of the stratified air flow by three-dimensional numerical computation. Okinotani et al. [4] studied transient formation characteristics of temperature-stratified flow in a horizontal water pipe with an injection of hot water from a hole in the pipe. However, there is no systematical research on this important flow mode. This motivated us to conduct the present more comprehensive analyses.

The improvements of the present study as compared with the former work are as follows: (1) In order to get a reasonable temperature distribution for highly temperature-stratified flow, usually lower-order schemes have been used. In the present study a high-resolution scheme was used and the reason why higher order schemes such as the QUICK scheme give physically unrealizable temperature solution can be seen from the present report. (2) In this study, we fixed the Reynolds number and changed the Grashof number to get a series of steady flow patterns. Then we can clearly observe the evolution process of the flow pattern from plug flow to highly temperature-stratified flow. (3) The effect of the Prandtl number on the flow pattern was studied. (4) The effect of the aspect ratio on the flow pattern was studied.

The present analyzed system is similar to that of [2]. Figure 1 shows the present model schematically. Cold fluid fills in a horizontal rectangular duct and the surrounding environment at a starting time. At some time, hot fluid flows into the duct continuously with uniform velocity at the inlet. Then hot fluid interacts with the cold fluid in the duct. It may be a common idea to presume that the hot fluid will push away the cold fluid out of the duct and will occupy the duct completely at the end. However, the experimental and numerical studies show that cold fluid at the lower part of the duct sometimes cannot be pushed out because of a buoyancy force. A secondary flow may occur at the exit of the duct, where hot fluid flows out at the upper part of the duct and cold fluid flows into the duct in the lower region. This is a temperature-stratified flow.

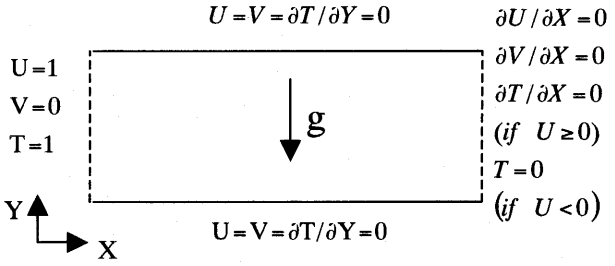

Fig.1 Description of the system with boundary conditions

Nomencalture

a	=coefficients in the finite-difference equation
b	=source term
g	=acceleration due to gravity [m/s^2]
Gr	=Grashof number $=g\beta(\theta_h-\theta_c)H^3/\nu^2$
H	=height of the duct [m]
L	=length of the duct [m]
p	=pressure [Pa]
P	=dimensionless pressure $=p/\rho u_0^2$
Pr	=Prandtl number $=\nu/a$,

Received October 27, 2000

* Postdoctoral fellow on leave from Xi'an Jiaotong University, Xi'an 710049, P. R. China

Re =Reynolds number $=Hu_0/\nu$
t =time [s]
T =dimensionless temperature $=(\theta-\theta_c)/(\theta_h-\theta_c)$
T_{av} =dimensionless average temperature $=\int TdA/A$
u =velocity component in the x direction [m/s]
u_0 =inlet velocity [m/s]
U =dimensionless velocity component in the x direction $=u/u_0$
U_{av} =dimensionless average velocity $=\int\sqrt{U^2+V^2}dA/A$
v =velocity component in the y direction [m/s]
V =dimensionless velocity component in the y direction $=v/u_0$,
x, y =spatial coordinate [m]
X, Y =dimensionless coordinate $=x/H,\ y/H$

Greek Symbols

α thermal diffusivity of fluid [m^2/s]
β volumetric coefficient of expansion [K^{-1}]
θ temperature [K]
ν kinematic viscosity [m^2/s]
ρ density [kg/m^3]
τ dimensionless time $=t/(H/u_0)$
Φ general variable

Subscripts

h highest temperature
c lowest temperature

Governing Equations and Boundary Conditions

Boussinesq assumption was made. Then the phenomena of the problem can be described by the following dimensionless governing equations:
Continuity equation

$$\frac{\partial U}{\partial X}+\frac{\partial V}{\partial Y}=0 \tag{1}$$

Momentum equation

$$\frac{DU}{D\tau}=-\frac{\partial P}{\partial X}+\frac{1}{\mathrm{Re}}\nabla^2 U \tag{2}$$

$$\frac{DV}{D\tau}=-\frac{\partial P}{\partial Y}+\frac{1}{\mathrm{Re}}\nabla^2 V+\frac{Gr}{\mathrm{Re}^2}T \tag{3}$$

Energy equation

$$\frac{DT}{D\tau}=\frac{1}{\mathrm{Re\,Pr}}\nabla^2 T \tag{4}$$

In the above equations, the following dimensionless parameters are introduced:

$Gr=g\beta(\theta_h-\theta_c)H^3/\nu^2$, $\mathrm{Re}=Hu_0/\nu$, $\mathrm{Pr}=\nu/a$,
$X=x/H$, $Y=y/H$, $U=u/u_0$, $V=v/u_0$,
$T=(\theta-\theta_c)/(\theta_h-\theta_c)$, $P=p/\rho u_0^2$, $\tau=t/(H/u_0)$

The duct was assumed to be filled with cold static fluid at the starting time, thus the initial condition is,

$$U=V=T=0 \qquad (\tau=0) \tag{5}$$

The boundary conditions are set as follows. At the inlet of the duct:

$$U=1,\ V=0 \tag{6}$$

$$T=1 \tag{7}$$

At the walls of the duct:

$$U=V=0 \tag{8}$$

$$\frac{\partial T}{\partial Y}=0 \tag{9}$$

At the outlet:

$$\frac{\partial U}{\partial X}=\frac{\partial V}{\partial X}=0 \tag{10}$$

$$\frac{\partial T}{\partial X}=0, \quad \text{if } U\geq 0 \tag{11}$$

$$T=0, \quad \text{if } U<0 \tag{12}$$

Numerical Approach

In former times the upwind-based lower order (LO) schemes have been used frequently because they are absolutely stable and possess boundedness. But in recent years, the usage of the LO schemes such as first-order upwind and power-law schemes for multi-dimensional viscous flows has received an ever-increasing criticism, especially for convection-dominant problems because of their well-known deficiency of being highly diffusive. For this reason, LO schemes were not used in this study. On the other hand higher order (HO) schemes, such as second-order upwind (SOU), central difference (CD) scheme and QUICK, can provide numerical results with higher accuracy but they suffer from the drawbacks of oscillatory or overshoot/undershoot behavior when the grid Peclet number is greater than some limit or when there exists a sharp change of profile in the computational domain. A QUICK scheme was tested by Ozoe et al. [2] to simulate the temperature-stratified flow and a negative temperature was found during the computational process for large Grashof number, which violates the physical principle. Thus these authors did not use the QUICK scheme for their final simulation, but rather used the Donor-Cell [5] scheme. Three HO schemes, i.e. QUICK, CD and SOU, were used to approximate the convection term in the present study. For $\mathrm{Re}=100$, $Gr=10^7$, $\mathrm{Pr}=5.6$ and $L/H=2$, negative temperatures were predicted by all the HO schemes as shown in Fig.2. This is because there exists

a sudden change in the temperature field at the inlet of the duct at the initial time. The physically meaningless negative values are undershoots. In order to overcome this shortcoming of HO schemes, many efforts have been made which lead to the development of bounded composite schemes, often called high-resolution (HR) schemes in the literature. High-resolution schemes can provide numerical solution with high accuracy while removing the overshoot/undershoot problems. Hence, in this study a HR scheme called MINMOD [6] was employed to evaluate the convection term. Fig.2 shows that the MINMOD scheme does not give unreasonable negative temperatures (undershoot), therefore it is appropriate for the calculation.

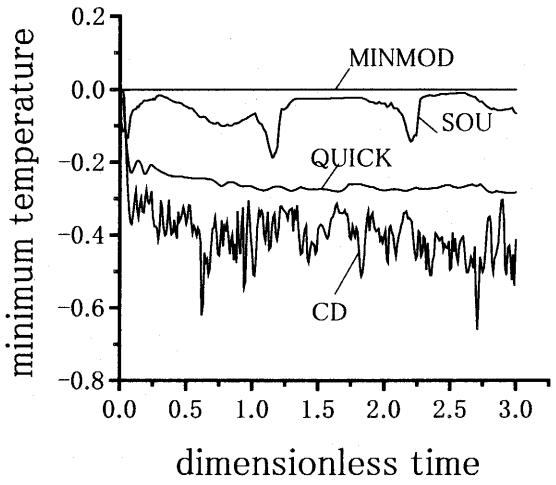

Fig.2 Comparison of different schemes for the temperature prediction for $Re=100$, $Gr=10^7$, $Pr=5.6$ and $L/H=2$

The governing equations were discretized by a control volume method on a staggered grid system as shown in Fig.3. The algebraic governing equations from the discretization can be written in a general form as follows.

$$a_P\Phi_P = a_E\Phi_E + a_W\Phi_W + a_N\Phi_N + a_S\Phi_S + b \qquad (13)$$

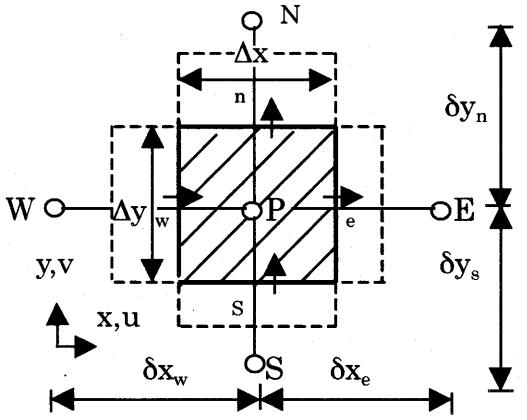

Fig.3 Control volume specification

The above discretized algebraic equations were solved by using a line-by-line alternating direction implicit (ADI) scheme. The pressure-implicit with splitting of operators (PISO) method proposed by Issa et al. [7] is adopted to deal with the linkage of pressure and velocity.

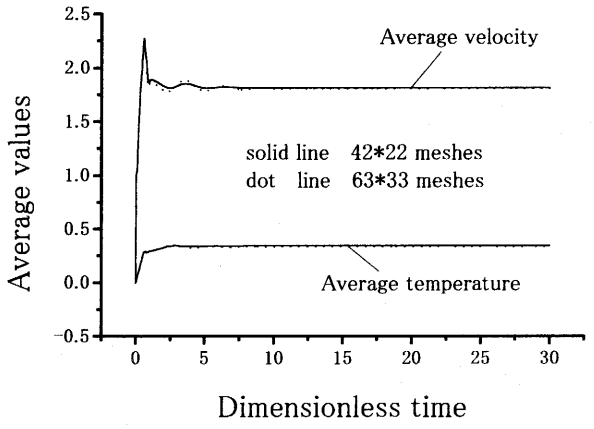

(a) Different grid numbers

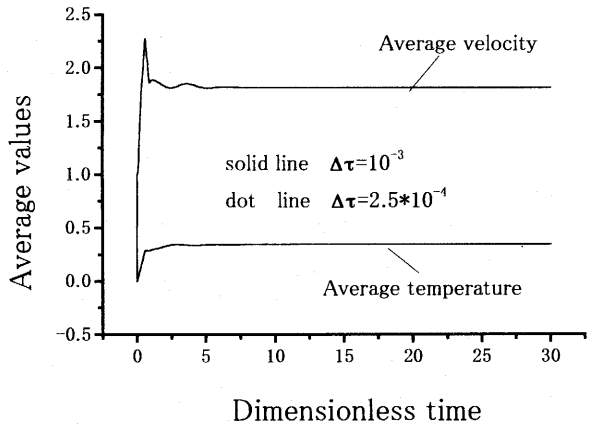

(b) Different time steps

Fig.4 Results independent of grid numbers and time steps for $Re=100, Gr=10^6, Pr=5.6$ and $L/H=2$

It is well known that numerical errors are related to mesh size and time step. In the following, the effects of mesh size and time step on the solution are discussed. Two uniform grid numbers 42×22 and 63×33 (in the X direction and the Y direction, respectively) were used for a typical case $Re=100, Gr=10^6, Pr=5.6$, $L/H=2$ and $\Delta\tau=10^{-3}$. Transient responses of the average velocity and average temperature are shown in Fig.4 (a). It is clear that the results obtained from two meshes are very close. For engineering application, the results obtained for grid 42×22 are accurate enough. In order to save computational time, in the following sections grids 42×22 were used except

where mentioned otherwise. Two dimensionless time steps 10^{-3}, 2.5×10^{-4} were adopted for $\mathrm{Re}=100$, $Gr=10^6$, $\mathrm{Pr}=5.6$ and $L/H=2$ with uniform grids 42×22. Figure 4 (b) shows that the transient responses from two different time steps agree with each other quite well. The difference is too small to be resolved in the graph. The larger time step was employed in the subsequent cases to reduce the computational time.

Computational Results

In this section, both transient and steady characteristics of stratified flow in a horizontal rectangular duct are presented. The transient process of two-dimensional temperature-stratified flow for water has been reported in [2]. In this study three typical transient replacements for air will be presented. Then the effects of the Grashof number, Prandtl number and aspect ratio on the steady stratified flow will be discussed.

Transient Replacement

In the following, three typical transient replacements for $\mathrm{Re}=100, \mathrm{Pr}=0.71$ and $L/H=2$ with different Grashof numbers $Gr=10^4$, 10^5 and 10^6 are shown.

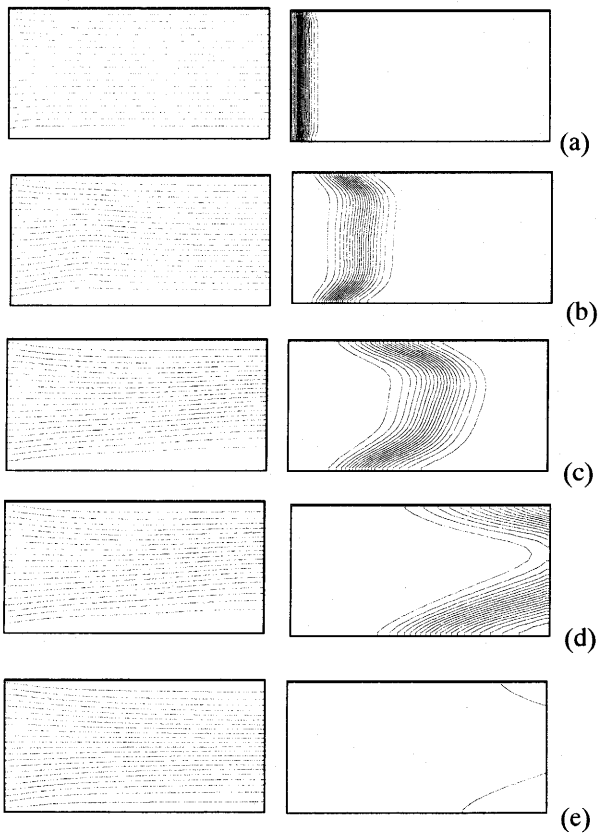

Fig.5 Transient contours of stream functions and temperature for $\mathrm{Re}=100$, $\mathrm{Gr}=10^4$, $\mathrm{Pr}=0.71$ and $\mathrm{L/H}=2$. $(a)\tau=0.1,(b)\tau=0.5,(c)\tau=1.0,(d)\tau=2.0,(e)\tau=6.0$

Figure 5 shows a series of instantaneous contours of stream functions and temperature for $Gr=10^4$. Since there exists a temperature difference between the inflow hot air and the cold air in the duct, a buoyancy force works for the air. The buoyancy force results in nonsymmetrical streamlines and nonsymmetrical temperature distributions with a higher temperature at the upper part of the duct. At $\tau=6$ the cold air is almost completely pushed out by the hot fluid. Then hot air continuously comes from the inlet and steadily flows out at the exit. No vortex is formed in the transient replacement process, because the action of the buoyancy force is very weak compared with the forced convection. In practice, for this case the dimensionless buoyancy force in Eq.(3) is $Gr/\mathrm{Re}^2=1$, which is small.

Figure 6 shows a series of instantaneous contours of stream functions and temperature for $Gr=10^5$. For this case the dimensionless buoyancy force in Eq.(3) is $Gr/\mathrm{Re}^2=10$, which indicates a stronger buoyancy force. Due to the stronger buoyancy force, a vortex is formed at the left lower part of the duct at time $\tau=0.5$ as shown in Fig.6 (b). The vortex continues to grow and move to downstream as depicted in Fig.6(c). At some time

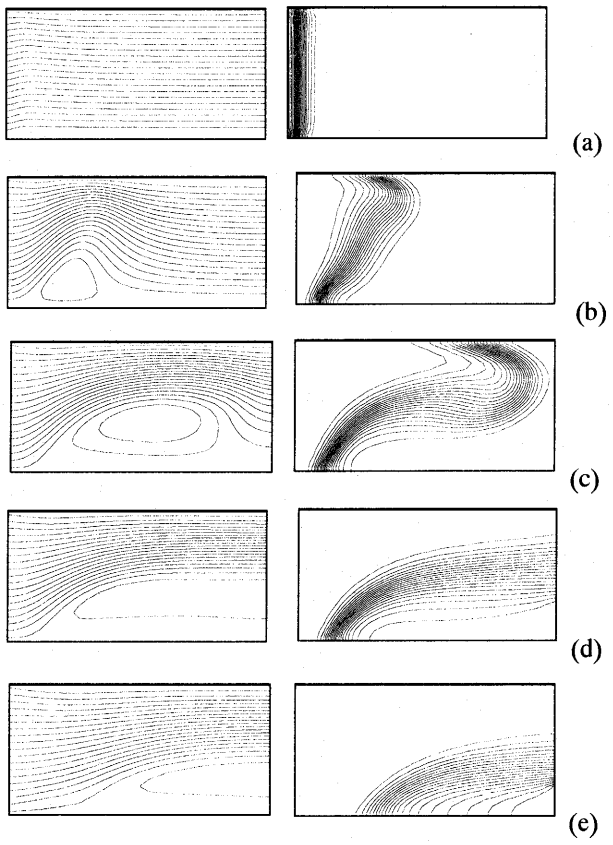

Fig.6 Transient contours of stream functions and temperature for $\mathrm{Re}=100$, $\mathrm{Gr}=10^5$, $\mathrm{Pr}=0.71$ and $\mathrm{L/H}=2$. $(a)\tau=0.1,(b)\tau=0.5,(c)\tau=1.0,(d)\tau=2.0,(e)\tau=6.0$

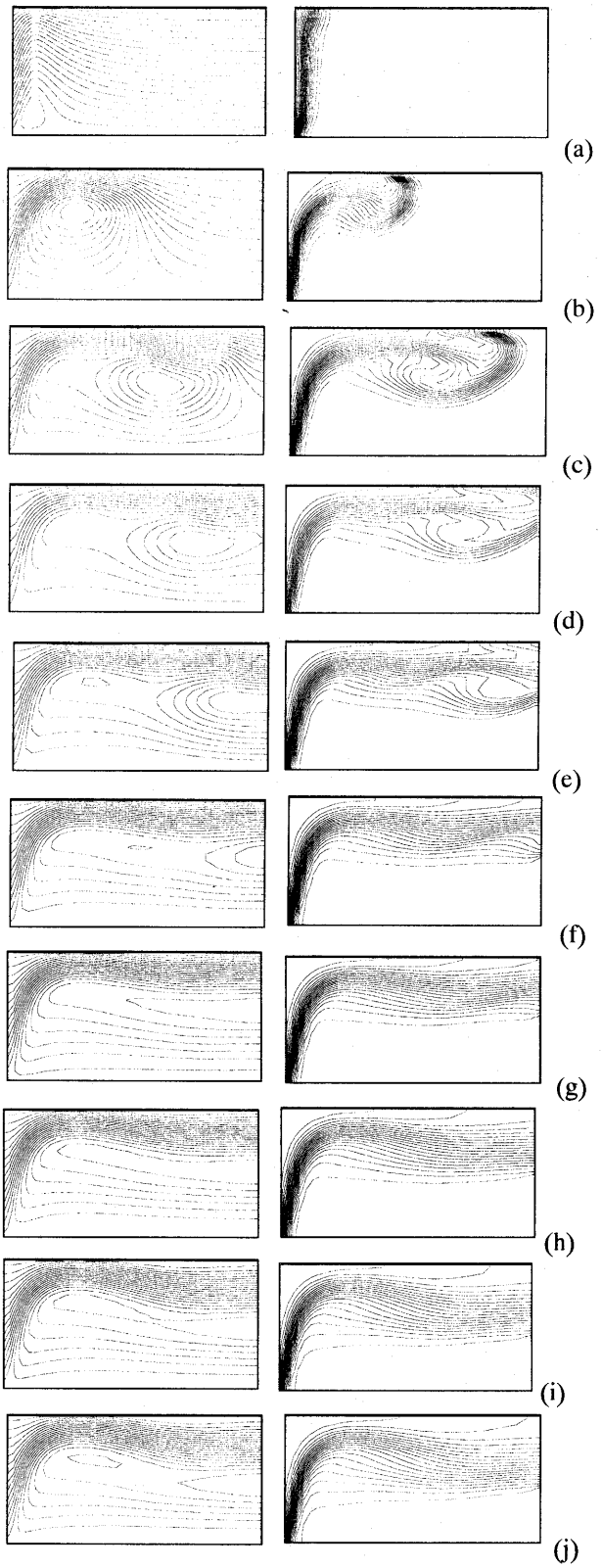

Fig.7 Transient contours of stream functions and temperature for Re=100, $Gr=10^6$, Pr=0.71 and L/H=2. (a)τ=0.1,(b)τ=0.3,(c)τ=0.5,(d)τ=0.6,(e)τ=0.7, (f)τ=0.9,(g)τ=1.0,(h)τ=2.0,(i)τ=5.0,(j)τ=10

between $\tau = 1$ and $\tau = 2$, the vortex arrives at the exit, thereby cold air comes into the duct. That means a secondary flow is formed at the exit. This secondary flow exists for many, many hours due to the stronger buoyancy force.

Figure 7 shows a series of instantaneous contours of stream functions and temperature for $Gr = 10^6$. For this case the dimensionless buoyancy force in Eq.(3) is $Gr/\mathrm{Re}^2 = 100$, which indicates a much stronger buoyancy force. A vortex is generated at time $\tau = 0.1$ as shown in Fig.7 (a). At some time between $\tau = 0.3$ and $\tau = 0.5$, the vortex arrives at the outlet. After $\tau = 10$, a steady flow is formed. In this case, a larger vortex is formed at the exit and the vortex extends to the region near the inlet. In addition, there is a small vortex inside the large vortex as shown in Fig.7 (j).

When comparing Figs.6 and 7, we can see that with the increase in the Grashof number, the vortex forms earlier, and grows and moves faster downstream.

Steady Stratified Flow

In our calculations, steady flows are achieved for all the studied cases at the end. Figs.8 and 9 show a series of stream functions and temperature contours at a steady state for an aspect ratio of 2 for air ($\mathrm{Pr} = 0.71$) and water

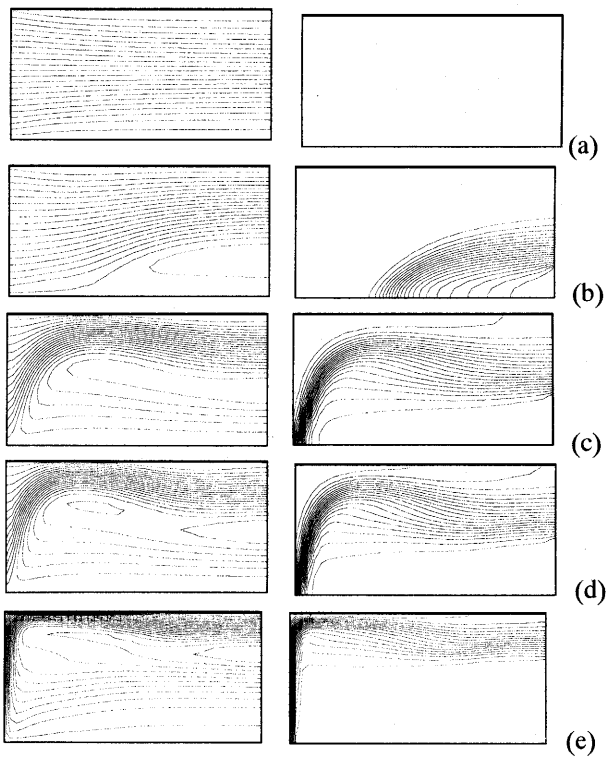

Fig.8 Contours of steady stream functions (left) and temperature (right) for Re=100, Pr=0.71, L/H=2 and different Grashof numbers for air. (a)$Gr=10^4$,(b)$Gr=10^5$,(c)$Gr=5\times10^5$,(d)$Gr=10^6$,(e)$Gr=10^7$.

$Pr = 5.6$, respectively. In these figures, the Reynolds number was fixed at 100. The Grashof number varies from 10^4 to 10^7. These figures are made to show the effects of the Grashof number and Prandtl number on the steady flow characteristics.

It can be seen clearly that the flow mode changes from plug flow to stratified flow with increase of the Grashof number for both air and water. There exists an inner vortex at $Gr = 10^6$ for air, and an inner vortex at $Gr = 5\times10^5 - 10^7$ for water. The center of the inner vortex moves from the lower part to the upper part of the duct with the increase in the Grashof number as shown in Fig.9 (c)-(e). The vortex at the exit becomes larger with the increase in the Grashof number as shown in Fig.8 (b)-(e) and Fig.9 (c)-(e). This makes the inlet flow change its flow direction slightly for low Grashof number but very steeply for high Grashof number upon flowing into the duct.

From Figs. 8 and 9, it can be seen that, at the same Reynolds number and aspect ratio, the critical Grashof number (at which plug flow becomes stratified flow) for air $(Pr = 0.71)$ is between $Gr = 10^4$ and $Gr = 10^5$, while for water $(Pr = 5.6)$ it is between $Gr = 10^5$ and $Gr = 5\times10^5$. This indicates the critical Grashof number is smaller for smaller Prandtl number under other identical conditions.

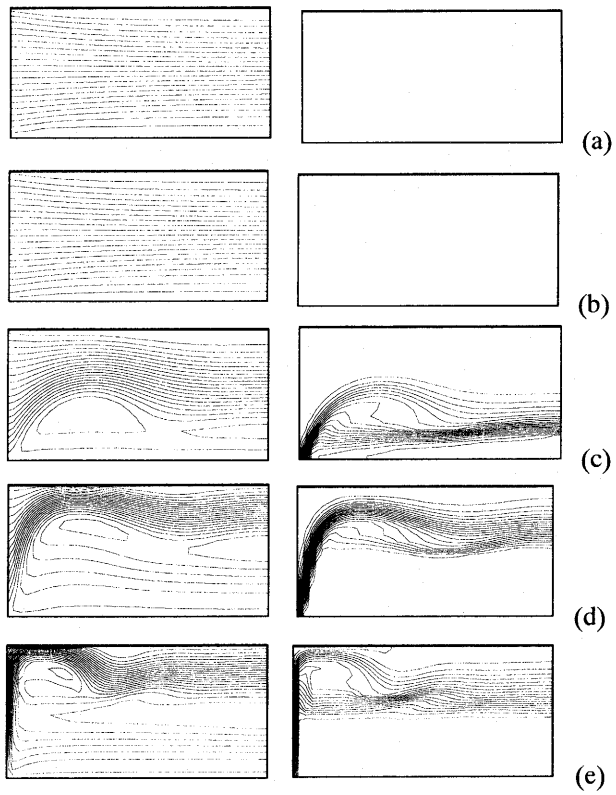

Fig.9 Contours of steady stream functions and temperature for Re=100, Pr=5.6, L/H=2 and different Grashof numbers for water. (a)Gr=10^4,(b)Gr=10^5,(c) Gr=5×10^5,(d)Gr=10^6,(e)Gr=10^7.

Figure 10 shows a series of contours of stream functions and temperature at a steady state for $Re = 100$, $Pr = 0.71$ and $Gr = 10^6$ with the aspect ratio varied from 2 to 16. The grid numbers used for aspect ratios 2, 4, 8 and 16 are 42×22, 84×22, 168×22 and 336×22 (in the X direction and the Y direction), respectively. The flow patterns and temperature distributions are similar for different aspect ratios.

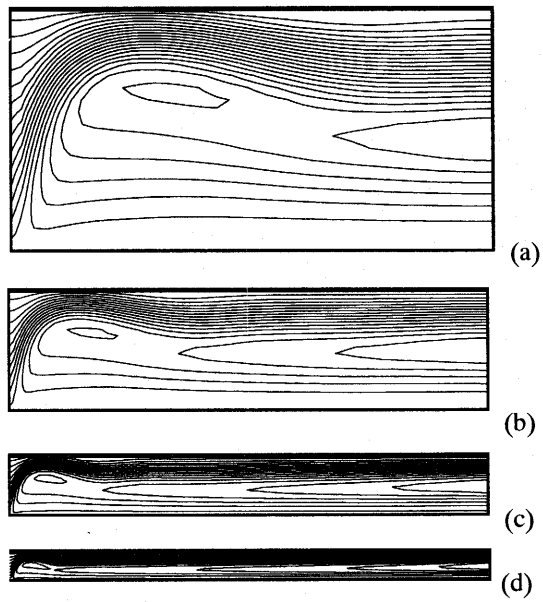

Stream function contours

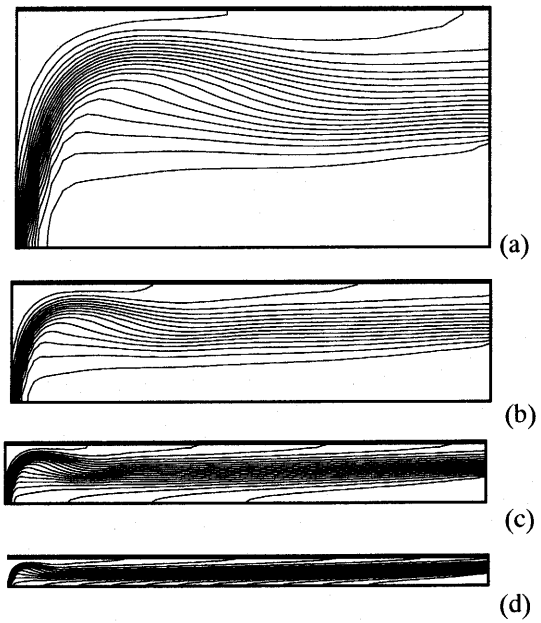

Temperature contours

Fig.10 Stream function and temperature contours at different aspect ratios for Re=100, Gr=10^6, Pr=0.71 (a)$L/H=2$,(b)$L/H=4$,(c)$L/H=8$,(d)$L/H=16$

Conclusion

The following conclusions can be drawn from the above calculations: (1) For non-isothermal duct flow, the buoyancy force should be taken into account. (2) For the present non-isothermal duct flow, the effect of the buoyancy force is weak for small Grashof numbers and it leads to a transient nonsymmetrical flow pattern. When Gr/Re^2 is small, the buoyancy force disappears and a steady isothermal plug flow is achieved. For mild Grashof number, buoyancy force becomes stronger, and a vortex is formed at the region near the inlet. The vortex grows and moves downstream; Finally a steady small vortex is formed at the exit. For high Grashof numbers a very large vortex is formed at the exit. (3) The critical Grashof number is smaller for air than for water under the same conditions. (4) For different aspect ratios, similar steady stratified flow patterns are obtained.

Acknowledgement

Bo YU is grateful for Dr. Toshio Tagawa for his helpful discussion.

References

1. Ozoe, H., Kanatani, K., Sato, T. and Sayama, H., The 46th Annual Meeting of the Society of Chemical Engineers, Japan. (1981), 638.
2. Ozoe, H., Mo, Y., Kanatani, K. and Sato, T., Chemical Engineering Science, 48(1993), 1557.
3. Mo, Y. and Ozoe, H., Proceedings of Joint conference of 3rd International Symposium of Heat Transfer and 5th International Symposium on transport Phenomena. Beijing, China, (1992).
4. Okinotani, T. and Ozoe, H., Proceedings of the 5th ASME/JSME Joint Thermal Engineering Conference, San Diego, California, (1999).
5. Gentry, R. A., Martin, R. E. and Daly, B. J., J. Comput. Physics, 1(1966).
6. Zhu, J. and Rodi, W., Comput. Methods Appl. Mech. Eng., 1.92(1991), 87.
7. Issa, R. I., J. Comput. Physics, 62(1985), 40.